Change in muscle fibre protein structure following salting process assessed by synchrotron deep UV fluorescence microspectroscopy

Saïd Abou El Karam, Duconseille Anne, Annie Vénien, Christine Ravel, Hugo Chauvet, Frederic Jamme, Matthieu Réfrégiers, Thierry Astruc

Food Chemistry 471 (2025) 142801

Contents lists available at ScienceDirect

Food Chemistry

journal homepage: www.elsevier.com/locate/foodchem

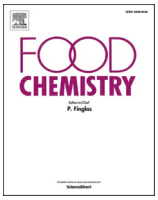

Change in muscle fibre protein structure following salting process assessed by synchrotron deep UV fluorescence microspectroscopy

Saïd Abou El Karam [a,*], Anne Duconseille [a], Annie Vénien [a], Christine Ravel [a], Hugo Chauvet [b], Frederic Jamme [b], Matthieu Réfrégiers [c], Thierry Astruc [a]

[a] INRAE, UR QuaPA, F-63122 Saint-Genès-Champanelle, France
[b] Synchrotron SOLEIL, L'Orme des Merisiers, Départementale 128, 91192 Saint-Aubin, France
[c] CBM CNRS UPR4301, rue Charles Sadron, 45071 Orléans, France

ARTICLE INFO

Keywords:
Synchrotron deep UV microspectroscopy
Muscle protein fluorescence
Muscle fluorophores
Muscle protein denaturation
Muscle fibre types
Brined meat

ABSTRACT

Samples of pork *teres major* muscle were salted and tumbled with 0.9 %, 1.3 % & 1.9 % sodium chloride respectively. The emission fluorescence (exc. 275 nm) of intramuscular connective tissue and of muscle fibre subtypes I, IIA and IIB-IIX was investigated by Synchrotron deep UV fluorescence microspectroscopy in order to characterize the change of the macromolecular structure of proteins. On emission spectra, tryptophan fluorescence was predominant and an additional peak assigned to dityrosine was detected around 395 nm. The fluorescence emission spectra vary depending on salt level both on intramuscular connective tissue and muscle fibres which subtypes were discriminated for one animal among the set of four. This result is encouraging in the perspective of developing sensors for meat evolution during the salting process. However, no noticeable prediction law linking the fibre autofluorescence to salt level could be deduced.

1. Introduction

Sodium chloride is added in meat processing as flavour enhancer, preservative, and texture-control agent. Moreover, salt brine improves the water-holding capacity of meat products (Offer & Knight, 1988). In "petit salé" which is a traditional French product made from pork shoulder, the salt content varies from 1.1 % to 1.9 % (0.17 to 0.35 M). Adding sodium chloride to meat increases the muscle tissue's ionic strength, resulting in the partial solubilisation of muscle fibre proteins, especially myosin, leading to the depolymerisation of thick filaments (Offer & Knight, 1988). C-protein, tropomyosin, troponin, and in a lesser extent, actinin and actin are also extracted by salt (Offer & Trinick, 1983; F. Y. Wu & Smith, 1987). Myosin starts to solubilise from 0.04 M NaCl in muscle extracts, (Offer & Knight, 1988; Ruusunen & Puolanne, 2005) and myofibrillar proteins have been shown to solubilise from 0.1 M NaCl in isolated myofibrils (Wu & Smith, 1987). The solubilisation of muscle fibre proteins is associated to change in their molecular structure (Abou El Karam et al., 2023; Böcker et al., 2006; Graiver et al., 2006; Wu et al., 2006). Böcker et al. (2006), using FT-IR microspectroscopy, showed that in situ muscle fibre protein started to denature as soon as it was incubated in brine containing 0.9 % NaCl (corresponding to 0.15 M NaCl) and the protein unfolding increased until 6 % NaCl.

Recently, we studied the denaturation of salted muscle protein extracts by exploiting the change in the autofluorescence of aromatic amino acids with the development of the protein conformation (Abou El Karam et al., 2023). The results demonstrated a change in emission fluorescence with salting from 0.9 % to 1.9 % NaCl but no obvious relationship of proportionality between salting and change in fluorescence could be established. However, a significant variability in the fluorescence response depending on individuals was observed. The threshold for salt denaturation of muscle proteins depends on the proportion of fibre type (Egelandsdal et al., 1994; Xiong, 1994) and on the organization of muscle tissue as a whole (Ruusunen & Puolanne, 2005). Our previous experiment (Abou El Karam et al., 2023) did not allow these two factors to be considered to the extent that the analyses were carried out on ground muscle without the possibility of targeting the microscopic tissue structure. Therefore, we hypothesise that the change in fluorescence could be induced by the ratio of muscle fibre types present in pig samples. The objective of the present study is to investigate the role of the muscle fibre types (metabolic and contractile) on the fluorescence emission spectra of pork samples prepared with different levels of salting ranging from 0.9 % to 1.9 % NaCl. A longer-term

* Corresponding author.
E-mail address: said.abou-el-karam@inrae.fr (S. Abou El Karam).

https://doi.org/10.1016/j.foodchem.2025.142801
Received 4 September 2024; Received in revised form 17 December 2024; Accepted 4 January 2025
Available online 6 January 2025

application aims to characterize the evolution of meat during salting in a fast, non-destructive, and operator-safe manner. This approach aims to enhance process control, optimize salt content, and reduce variability in meat product quality.

To perform these measurements, we used Synchrotron deep UV (S-DUV) fluorescence microspectroscopy. This technique enabled us to record, on label free thin muscle sections, the intrinsic fluorescence emission spectra for different individual muscle fibres previously identified on their subtype by histology (Chagnot, Venien, et al., 2015; Chagnot, Vénien, et al., 2015). The spectra were acquired in muscle fibres identified on their subtype and in intramuscular connective tissue before and after the salting process. Multivariate analyses enabled us to evaluate the effect of salt on the autofluorescence response of different muscle components.

2. Material and methods

2.1. Animals

The present study was carried out on a subset of 4 pigs identified An1 to An4. The animal subset corresponds to P5, P6, P7 and P9 pigs from a set of nine animals used in a previous study (Abou El Karam et al., 2023). The experiment was performed on *teres major* (TM) muscle from four 6-month-old, female Pietrain x (Large White x Landrace) pigs whose average carcass weight was 91.90 ± 7.29 kg (Table 2).

The pigs were slaughtered in a commercial abattoir approved for the slaughter of animals intended for human consumption and respecting the rules of respect for animal welfare in accordance with European regulations (EU 1099/2009, 853/2004 & 2017/625 regulating the hygiene rules applicable to foodstuffs of animal origin and to the health and welfare of animals among others).

Lean meat content (LMC) percentage was determined with a CSB Image-Meater following European Commission guidelines (European Commission, 2013) and pH, which reflect the muscle postmortem metabolism kinetic (Adzitey & Nurul, 2011; Bendall, 1973), was measured on the *semimembranosus* muscle using a pH-meter (Sydel, France) equipped with a combined penetration electrode Xerolyt® (MettlerToledo, Switzerland) for solid foods.

2.2. Muscle sample processing

At 24 h *postmortem*, the TM muscle (approximately 150 g) was extracted from each half carcass and transported for about 4 h in a cooler at 4 °C ± 2 °C to the laboratory. About 20 g of each muscle was sampled and assigned to 0.9 % NaCl (Physiological serum in order to respect the osmolarity of fresh muscle and identified as C for control samples), 1.3 %, and 1.9 % NaCl respectively. The last two (1.3 % & 1.9 %) contained 0.05 % sodium ascorbate to prevent lipid oxidation and to meet French professional practices. The amount of brine required to achieve the desired salt content was calculated based on the mass of each muscle sample. Each sample was placed with its assigned brine in a vacuum pouch (PA-PE 20/70, 135 mm × 180 mm) and vacuum-sealed using a Gastrovac machine (Multivac). The samples were tumbled for 16 h between 0 and 4 °C at 4 rpm. All samples were then stored at 4 °C for 48 h to allow salt diffusion within the muscle tissue (Table 1).

Table 1
Detail of the salt treatments applied to the muscle samples.

#	Processing	NaCl (%)	Na ascorbate (%)	Tumbling
1	C	0.9	0.00	Yes
2	1.3 %	1.3	0.05	Yes
3	1.9 %	1.9	0.05	Yes

2.3. Determination of salt content in muscle samples

NaCl content was determined by ion chromatography (Mirade et al., 2020). Briefly, a 0.5 g of sample was ground, homogenised in pure water and centrifuged at 14000 rpm for 20 min. The sodium content was determined in the supernatant by ion exchange chromatography (850 Professional IC METROHM, Switzerland, equipped with a Metrosep C4-silica column grafted with carboxylic groups and a conductometric detector) from a calibration curve.

2.4. Light microscopy (histology and UV microspectroscopy) section preparation

From each condition, sample cubes of 1 cm were cut according to the direction of the muscle fibres. The samples were frozen in cooled isopentane (−160 °C) chilled by liquid nitrogen (−196 °C), and stored at −80 °C until analysis. Thin serial fibre cross-sections (10 µm-thick) were sliced at −25 °C using a cryomicrotome (Leica CM 1950, Leica Biosystems, Nussloch, Germany), and collected on glass slides for histological stains, and on quartz coverslips (ref. CNO.WIN-30-0.17-UV, Laser Components, 92,190 Meudon, France) for S-DUV microspectroscopy acquisitions. Sections for histochemical analysis were stored at 4 °C until staining had taken place. Sections for S-DUV microspectroscopy were stored at −80 °C under vacuum until they were analysed on the Synchrotron beamline.

2.5. Histochemistry staining

Sections were stained with hematoxylin-eosin-saffron (HES) to reveal general structure, and with picro-Sirius-red to reveal perimysial and endomysial collagen. After staining, the slides were mounted with a synthetic resin (Eukitt, Kindler GmbH & Co, Freiburg, Germany) in order to protect the sections over time. Observations and image acquisition were performed on an optical transmission microscope coupled to a digital acquisition kit (Olympus BX61 microscope, Olympus DP 71 digital camera and Cell F software, Olympus France SAS, Rungis, France).

2.6. Identification of muscle fibre subtypes

The muscle fibre types were delineated by determining actomyosin ATPase activity after incubating sample sections in acid solution (pH 4.45) according to Guth and Samaha (1969). The staining carried out on the control muscle samples displayed type I fibres in black revealing high ATPase activity, type IIA fibres in white revealing a loss of ATPase activity, and type IIB-IIX fibres in dark grey revealing partial ATPase activity (Fig. 1). However, the low contrast difference between IIB-IIX fibres and IIA fibres in some treated samples led us to implement an immunohistofluorescence labelling technique to highlight muscle fibre outlines and confirm fibre identification.

This muscle fibre typing technique uses monoclonal antibodies specific to myosin heavy chain (MyHC) isoforms characteristic of the cell type according to Chagnot, Venien, et al. (2015). Slow and fast MyHC were identified using BA-D5 mouse monoclonal antibodies (AGRO-BIO France). The BA-D5 MyHC antibodies were visualized using an Alexa Fluor 488 labelled goat anti-mouse IgG secondary antibody (A 11001, Invitrogen). Type I fibres display relatively higher fluorescence compared to IIB-IIX fibres which have a lower fluorescence, while type IIA fibres do not fluoresce (black on the immunohistofluorescence image). The muscle fibre outline was highlighted using a rabbit anti-laminin primary polyclonal antibody (L9393 Sigma), and a goat anti-rabbit IgG Cy3-labelled secondary antibody (111–165-008, Jackson) where in the resulting images, the laminin is revealed in orange. Myofiber types, identified with both histoenzymology (ATPase staining) and immunohistochemistry, were then manually localized on the unstained serial sections prepared for S-DUV microspectroscopy measurements.

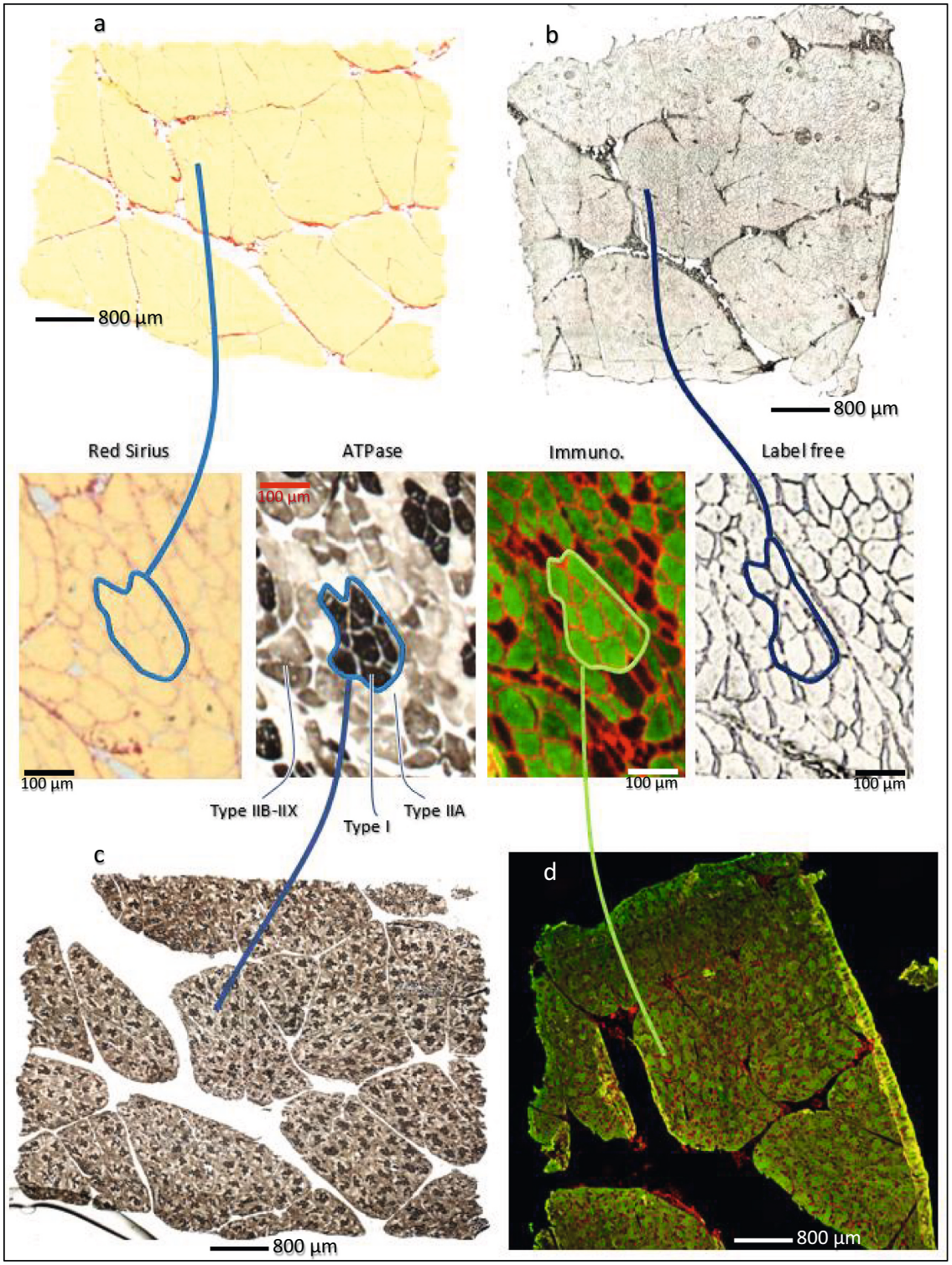

Fig. 1. Muscle fibre type identification from histology images. Sirius-red staining (a) highlights the muscle fibres in yellow and the intramuscular connective tissue (IMCT) in red. Muscle fibre types were identified both by acidic pre-incubation ATPase staining (c) and immunohistofluorescence (d) of myosin heavy chains (MyHC) isoforms. ATPase staining identifies type I, type IIA and types IIB-IIX by black, white and grey colour respectively on control muscle samples. Independently of the salt content, immunohistofluorescence identified extracellular matrix in orange and muscle fibres in green (d); fibres of type I fluoresce strongly, while IIA fibres fluoresce moderately; those of IIB-IIX do not emit any fluorescence (black). These data enabled identification of muscle fibre types on label free sections (b) thanks to the muscle structure and muscle fibre morphology. (For interpretation of the references to colour in this figure legend, the reader is referred to the web version of this article.)

2.7. Deep UV microspectroscopy spectra acquisitions

The UV measurements were performed using the inverted micro-spectrofluorometer, so-called Polypheme, of the imaging branch of DISCO beamline at the Synchrotron SOLEIL (Giuliani et al., 2009; Jamme et al., 2010; Réfrégiers et al., 2012). UV monochromatized light (at 275 nm) was used to excite label free thin tissue sections, through a 40× ultrafluar immersion objective (N.A 0.65, Gly, Zeiss, Germany). Fluorescence emission spectra were acquired from 284 to 555 nm and recorded with 0.5 nm spectral resolution, with a spot size of 2 μm and an acquisition time of 1 s for each position. Positions of spectra acquisition spots were selected manually in targeting the IMCT cells and each of the 3 muscle fibre types i.e. I, IIA and IIB-IIX. Note that fibre types IIB and IIX were binned in the same group because they are not discriminable on our histological images.

The spectra spots were chosen spaced several μm apart inside each analysed tissue cell. Furthermore, in the IMCT, the scanned areas were chosen to be wide enough to integrate the scanning light beam. The spectrometry bench acquires the spectra by setting the area to be automatically scanned (cartography mode) or by manually indicating, on the sample sections, the targeted locations to be analysed. Typically, about 3 spectra per muscle cell were acquired in10 cells of each of the 3 cell types and IMCT, which led on average to (3 × 10 × 4) 120 spectra for each of the 12 muscle sections given by the 3 NaCl treatments and the 4 animals. This on average, however the acquisition zones were expanded whenever possible to collect more spectra. This approach helps account for non-compliant data, often affected by noise or distortions, and ensures to have enough data for the analysis reliability.

2.8. Spectra and signal pre-processing

Spectral data processing was carried out using software tools developed in the MATLAB® environment (The MathWorks Inc., MATLAB R2019a [9.6.0], Natick, Massachusetts). Pre-treatment processing of spectra was performed using homemade MATLAB programs. The baseline spectrum was set by subtracting the minimum value from the spectrum amplitude. Removal algorithm of spikes and dead pixels was based on derivative and spline interpolation. To reduce signal noise, spectra were smoothed using Savitsky-Golay algorithm. Spectra were finally normalised using the min-max algorithm. All these pre-treatments generated no notable deformations or distortions on the spectra (see Fig. SD1).

2.9. Statistical analysis

Principal component analysis (PCA) was performed to explore and discriminate samples (in scatter plots) and to identify the wavelength ranges (in loading plots) that contribute most to sample separation. The ANOVA was calculated for each wavelength of the spectra and the result was plotted in what we called anovagram. The power of sample discrimination of a range of wavelengths was estimated by using the level of significance given by low p values (< 0.05) associated with high F values. The anovagram was used here to estimate the significance and therefore the relevance of sample discrimination at each wavelength and for a given factor. The anovagram plot displays the Fisher's F & p values where in plots only p values < 0.05 are displayed and represented by 'x' at the associated wavelength. To refine the ANOVA results, Tukey's post hoc test was used to highlight differences between sample groups. ANOVA & PCA were performed on emission fluorescence spectra to investigate effects of sample salt processing ($n = 3$), type of muscle cells & IMCT ($n = 4$) and animal (n = 4) factors.

3. Results and discussion

3.1. Carcass traits and muscle pH

Carcass traits i.e. initial pH (pH_1), ultimate pH (pH_u) and salt levels are provided in Table 2. There are significant differences in carcass weight among the animals (81.8–98.8 kg), with An1 and An4 carcasses being the heaviest and the lightest, respectively.

An3 and An4 show pH_1 values below 6.10, reflecting a fast *postmortem* metabolism (Bendall, 1973). This accelerated *postmortem* metabolism can be a consequence of high physical activity or animal stress prior to bleeding (Astruc et al., 2002; Monin et al., 1973; Terlouw et al., 2021). Unfortunately, we do not have any data on the progress of the slaughter stages preceding bleeding. Note that the An2 stands out because of high pH_1 & pH_u compared to the 3 other animals, which likely reflects stress and/or intense muscular activity in hours preceding slaughter (Astruc & Terlouw, 2023).

3.2. Muscle sodium chloride content

NaCl rates measured in brined samples (1.3 % and 1.9 %) revealed higher variability than in control ones (C) (see SD in Table 2). This salt content variability is likely due to a heterogeneity in salt distribution since the structure and lipid composition of muscle tissue impact the salt diffusion (Lebert & Daudin, 2014). As experimental animals demonstrated some variability in weight and LMC, it could be assumed that their carcasses had variations in muscle composition, especially in fat content, likely to contribute to the salt distribution heterogeneity.

3.3. Histology

A quantification of the *teres major* fibre type composition assessed from the ATPase images of the unsalted samples (Fig. 1) gave 30 % of type I, 26 % of type IIA and 44 % of IIB-IIX fibres ($n = 595$ muscle fibres). As expected, immunohistofluorescence confirmed the results of ATPase staining, thus ensuring the identification of fibre types, and in particular type IIB-IIX fibres which show moderate fluorescence while IIA fibres do not fluoresce (Fig. 1). Looking ATPase staining, the reduced contrast between IIA fibres and IIB-IIX fibres in some salted samples could be attributed to decreased ATPase activity, resulting from partial denaturation due to a localized increase in ionic strength (Dancker & Hasselbach, 1971), itself linked to a higher sodium chloride content.

3.4. UV microspectroscopy results

3.4.1. UV microspectroscopy of control samples (C)

Whether the spectra were acquired in connective tissue or muscle fibres, the mean emission spectra clearly show two main contributions

Table 2
Carcass characteristics, *postmortem* pH and measurements of salt content in muscle samples. An1 to An4 correspond to the 4 studied animals. LMC refers to lean meat content percentage. pH_1, pH_u: initial and ultimate pH measured respectively at 45 min and at 24 h *postmortem*. C, 1.3 % and 1.9 % correspond to salt level classes. Salt content was measured in muscle samples, using the 850 Professional IC chromatogram, where each measured NaCl value was binned into its associated NaCl class. From the Tukey post-hoc test, different letters mean significant differences between NaCl classes for $p < 0.01$.

	Carcass traits				NaCl class/content (%)		
Animal #	Mass (kg)	LMC (%)	pH_1	pH_U	C	1.3 %	1.9 %
An1	98.8	63.50	6.16	5.68	0.14	1.43	2.05
An2	95.0	63.10	6.45	6.16	0.18	1.30	1.91
An3	92.0	61.60	6.07	5.64	0.18	1.16	2.06
An4	81.8	62.20	5.99	5.65	0.19	1.14	1.79
Average	91.90	62.60	6.17	5.78	0.17^{a}	1.26^{b}	1.95^{c}
SD	7.29	0.86	0.20	0.25	0.02	0.14	0.13

located at 340 nm and around 395 nm respectively (Fig. 2, a) and a slight shoulder at 302 nm. This last fluorescence peak at 302 nm is assigned to tyrosine (Chagnot, Venien, et al., 2015; Jamme et al., 2013).

The emission fluorescence peak at 340 nm can be reasonably assigned to tryptophan whose fluorescence emission varies from 330 to 360 nm in biological tissues (Jamme et al., 2013) although mostly observed at 332 nm in skeletal muscle and muscle extracts (Abou El Karam et al., 2023; Chagnot, Venien, et al., 2015; Sahar et al., 2009). This red shift in the tryptophan fluorescence peak could be related to a slightly different muscle composition, since tryptophan fluorescence is influenced by its molecular environment (Lakowicz, 2006; Valeur & Berberan-Santos, 2001). A peak at 410 nm (exc. 275 nm) was observed by Chagnot et al. (2015) which is close to the 395 nm peak found in the present study; but in a previous study (Abou El Karam et al., 2023) no peak around this wavelength (395 nm) was observed on the pig *teres major* extracts analysed with a laboratory spectrofluorometer equipped with an internal light source (see Fig SD4). Additional measurements, on *teres major* and on other muscle samples, which were performed in our laboratory and in Synchrotron laboratories as well (results not shown) showed that this peak around 410 nm only appeared following micro-spectroscopy measurements. It therefore seems obvious that this peak is only evidenced by the focused beam provided by microspectroscopy.

In animal tissues, a fluorescence emission at 393 nm is assigned to pyridoxine. But the maximum emission of pyridoxine is obtained when excited with both wavelengths 252 and 322 nm (Jamme et al., 2013) while it is weakly excited under our 275 nm excitation conditions. Possibly, the tryptophan emission fluorescence (maximum fluorescence at 340 nm, which is close to 322 nm) could excite pyridoxine which in turn fluoresces around 393 nm (Fig.2, a). However, this hypothesis is inconsistent with the highest fluorescence emission observed in intra-muscular connective tissue compared to muscle fibres ($p < 0.01$, Fig. 2, b) and also evidenced by the PCA score plot (Fig. 2, c). Indeed, IMCT is composed of 90 % collagen which is devoid of tryptophan (Bailey & Light, 1989). The dityrosine trail is more relevant. Excited at 280 nm (close to our 275 nm excitation conditions), dityrosine emits at 405 nm (Duconseille et al., 2018). Dityrosine crosslinks are present both in collagen (Waykole & Heidemann, 1976) and in other proteins (Curry et al., 2020; Huggins et al., 1993; Kato et al., 2001; Ushijima et al., 1984). Therefore, the peak observed at 395 nm both in the muscle fibre and in the extracellular matrix (IMCT) is likely to come from the dityrosine autofluorescence. The higher fluorescence emission (around 400 nm) in the extracellular matrix compared to the signal of muscle fibres ($p < 0.01$, Fig. 2, a & b) can be explained by an accumulation of fluorescence emission from dityrosine and other collagen cross-links which also emit in this wavelength band (Jamme et al., 2013) especially the pyridinoline and deoxypyridinoline which emits at 395 nm

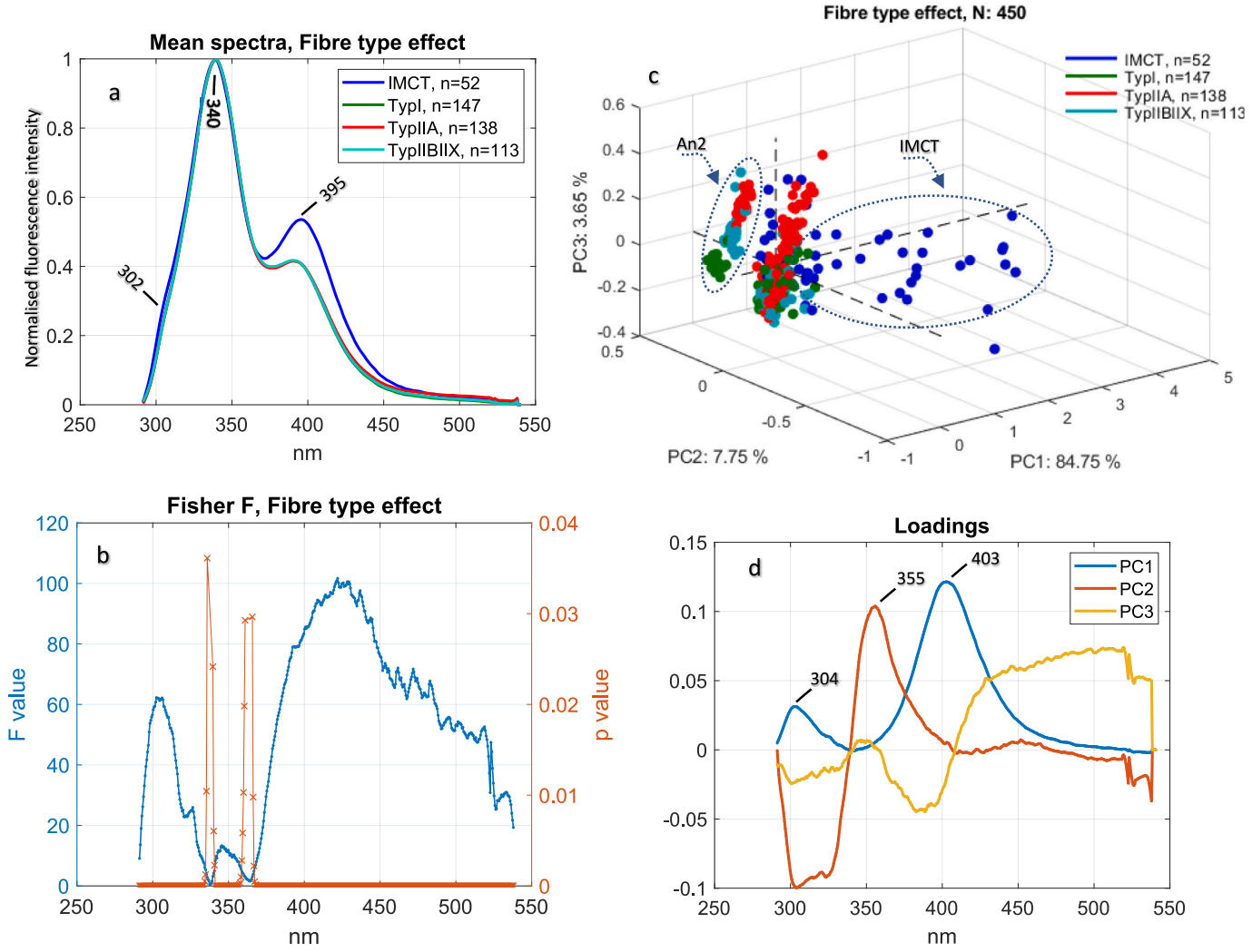

Fig. 2. Control samples of 4 animals with data of IMCT and 3 fibre types. Normalised mean spectra (a); anovagram plots of the Fisher's F & p values (b) where only p values < 0.05 are represented by 'x' at the related wavelength (red curve); PCA score plot (c); PCA loadings (d) for the three 1st principal components PC1, PC2 & PC3. (For interpretation of the references to colour in this figure legend, the reader is referred to the web version of this article.)

when excited at 297 nm (Karim & Bouxsein, 2016).

PCA does not separate fibre types from each other except for An2 animal on PC3 (Fig. 2, c). An2 is the only one which displayed a significantly high ultimate pH (6.16 compared to 5.66, mean pH of the 3 others, Table 2). Surprisingly, in the study of Chagnot, Venien, et al. (2015) who were able to discriminate the fibre type on rat EDL *(extensor digitorum longus*) and *soleus* muscles using the same approach on the same Synchrotron beamline, the ultimate pH of rat muscles was also higher than 6.0. It is possible that the amplitude of pH drop, which affects the physicochemical environment of muscle cells, can modulate their fluorescence emission. The intensity of fluorescence emission is influenced by pH variations (Lakowicz, 2006). In our study, pH variations of about 0.5 units between the extremes are too small to induce too large changes in fluorescence emission. Additional research with larger numbers of samples is needed to get a clearer answer to this question. Tumbling is not responsible for the An1, An3 and An4 non-separation of fibre types based on autofluorescence spectra analysis as shown by measurements carried out on An1 samples that gave the same results with or without sample tumbling (results not shown). The absence of tumbling effect was also seen in previous results on muscle extracts (Abou El Karam et al., 2023).

As we have a significant separation of the IMCT compared to the muscle fibres which the subtypes do not separate well (Fig.2 & Fig. 3), we considered relevant to remove the IMCT from the analysis as it could mask a possible fibre subtype effect. By excluding the IMCT data, the PCA exhibits a separation of individual pigs (see supplementary data Fig. SD3) as already seen in a previous study (Abou El Karam et al., 2023) on muscle extracts from the same samples.

3.4.2. *Effect of the salting/tumbling process on muscle fluorescence emission*

PCAs and ANOVA analyses, display a strong and significant ($p < 0.01$) differentiation of IMCT compared to muscle fibres as previously observed on the unsalted control muscles (Fig. 3, b, d & g).

This difference in fluorescence spectra between muscle fibre types and IMCT is maintained after salting as shown by the PCA score plot

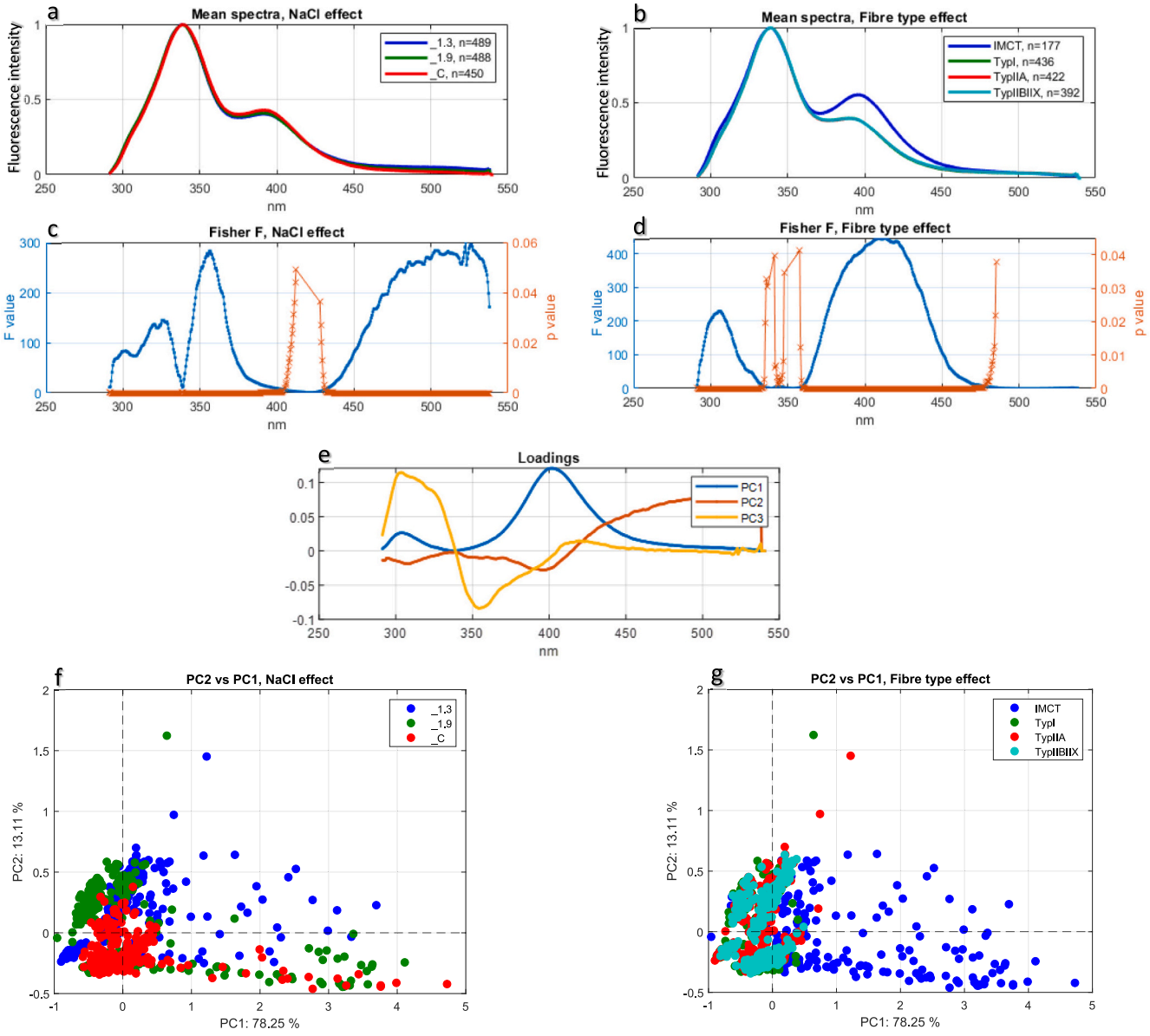

Fig. 3. Normalised mean spectra of 4 animals, according to NaCl and fibre type factors, are presented in the top graphs (a & b). Anovagrams, resulting from ANOVA calculations are shown according to NaCl (c) and fibre type (d) factors. The loading plot is presented in the graph 'e'. The two lower graphs show PCA score plots coloured according to NaCl (f) and fibre type (g) factors.

(Fig. 3, g), and particularly confirmed in the 365–455 nm range by the Fisher's values ($p < 0.01$) and PC1 loadings (Fig. 3, d & e).

To refine the effect of salting on the myofibers only, IMCT was removed from the analyses and the corresponding results are presented in Fig. 4. The fluorescence intensities at wavelengths of 302, 355 and 395 nm pointed in the loadings graph (Fig. 4, c), were identified as being predominant in the separation of sample groups. ANOVA highlighted that control samples are significantly different ($p < 0.01$, Fig.4, b) from samples of the two salt concentrations 1.3 % and 1.9 % for the three tested wavelengths (Table 3).

Salted samples displayed a higher intensity at 302 nm and a lower intensity at 355 and 395 nm (Table 3) reflecting a blue shift of NaCl treated samples compared to control ones, as shown by the spectra superposition (Fig. 4, a & Fig. SD5). This blue shift could be a salt consequence on environment of tryptophan buried in the protein structure (Lakowicz, 2006; Vivian & Callis, 2001).

The PCA analysis shows a partial sample separation according to NaCl contents (Fig. 4, d) likely due to interindividual animal effect as highlighted on control samples (see end of section 3.4.1 UV microspectroscopy of control samples) and according to previous results on pig *teres major* muscle extracts (Abou El Karam et al., 2023). However, the fluorescence intensities at 355 and 395 nm of 1.3 % and 1.9 % samples were significantly ($p < 0.01$) different although the differences were very low (0.006 a.u., Table 3). The autofluorescence of the different fibre types is not affected ($p > 0.01$) by the salting process (Fig. SD2, a, b & c). The ANOVA and PCA (Fig. SD2, d, e & f) confirm a slight but significant individual animal variability as previously evidenced on the control samples (Fig. SD3).

The significant interindividual animal variability shown on salt treated samples (Fig. SD2, a, e & f) and on control ones (Fig. SD3) encouraged us to carry out analyses using individual animals and excluding the IMCT data in order to focus on the muscle fibres so that we could investigate the subtype effect.

On PCA scatter plots for each animal, the autofluorescence spectra separate the different NaCl concentrations quite well, while fibre types remained mixed except for the control samples of the An2 (Fig. 5, 2nd raw, 3rd column), as previously stated (Fig. 2, c).

Table 3
Normalised fluorescence intensities (mean ± SEM) for the 3 relevant wavelengths and for C, 1.3 % and 1.9 % samples. In each column, different letters indicate significant difference for $p < 0.01$.

Wavelength	302 nm	355 nm	395 nm
C	0.178 ± 7.46E-04 [a]	0.666 ± 1.07E-03 [a]	0.410 ± 1.05E-03 [a]
1.3 %	0.197 ± 7.05E-04 [b]	0.639 ± 7.73E-04 [b]	0.383 ± 1.87E-03 [b]
1.9 %	0.197 ± 5.41E-04 [b]	0.645 ± 5.96E-04 [c]	0.377 ± 1.05E-03 [c]

Overall, the PCAs calculated on the fluorescence spectra did not reveal any separation of samples according to fibre types. However, they show a clear distinction of samples according to salt levels for all four animals, although this separation seems less marked for An3. A detailed examination of the PCAs of this animal (Fig. 5, 2nd column and 3rd column) reveals that samples from the 1.3 % and 1.9 % NaCl classes are clearly differentiated. In contrast, those of class C, associated with type IIA fibres, demonstrated a significant dispersion and overlap with the other two classes (NaCl). At this stage, we can only advance a hypothesis regarding the variability of autofluorescence of IIA fibres, which could be explained by a genetic characteristic. The predominant emission bands in the separation of the groups are mostly located in the regions close to 360 and 400 nm (PC2) and around 400 nm (PC1) for An1 to An4 with a slightly different PC1 pattern for An2. As previously discussed on the interpretation of unsalted samples, the fluorescence emission from muscle fibres around 400 nm could be assigned to dityrosine (Curry et al., 2020; Huggins et al., 1993; Kato et al., 2001; Ushijima et al., 1984) and pyridoxine (Jamme et al., 2013).

The emission zone going from 400 to 550 nm could be attributed to NADH which is excited in the deep UV at 260 nm (Dubreil et al., 2023; Jamme et al., 2013). These variations in spectral fluorescence emission around and beyond 400 nm were not observed on ground muscle

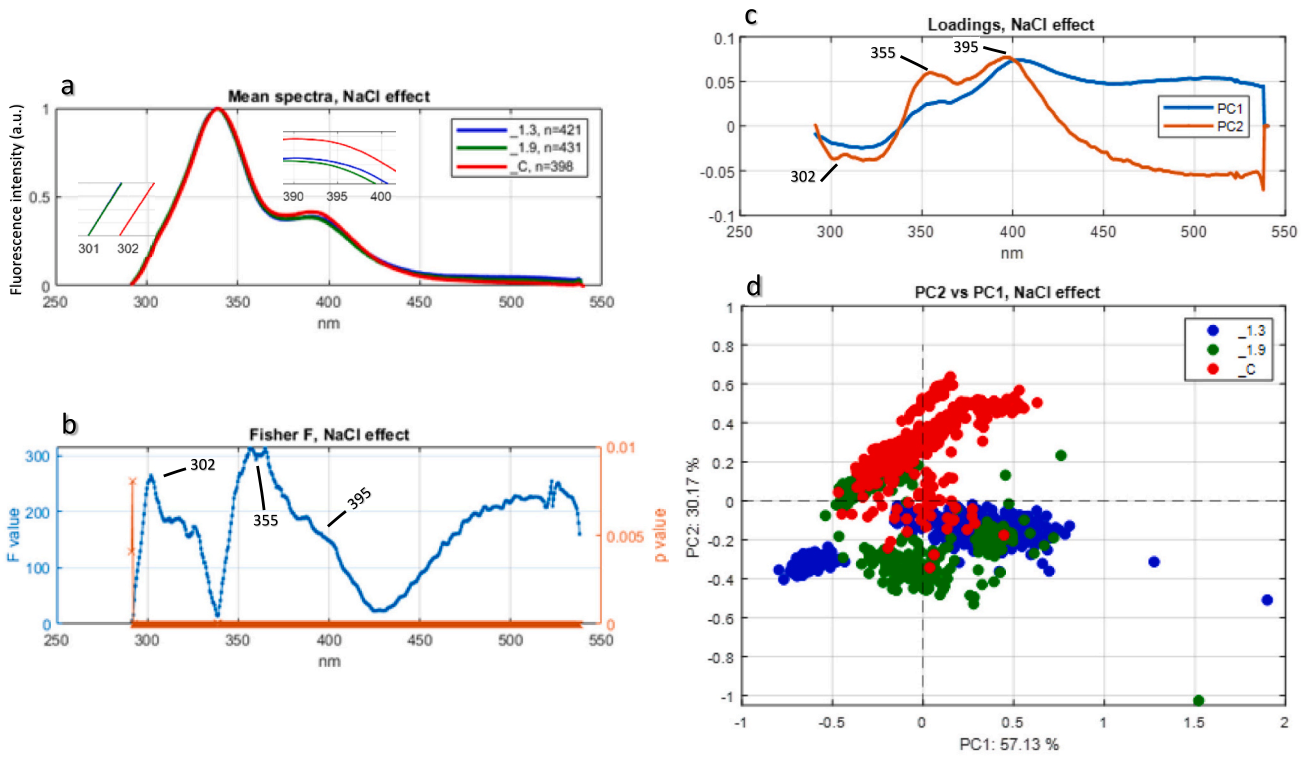

Fig. 4. Results from data of 4 animals, 3 fibre types and 3 NaCl levels. Normalised mean spectra of NaCl factor (a); anovagram plots of Fisher's F and *p* values according to NaCl factor (b); PCA loadings (c) and score plots coloured according to NaCl factor (d).

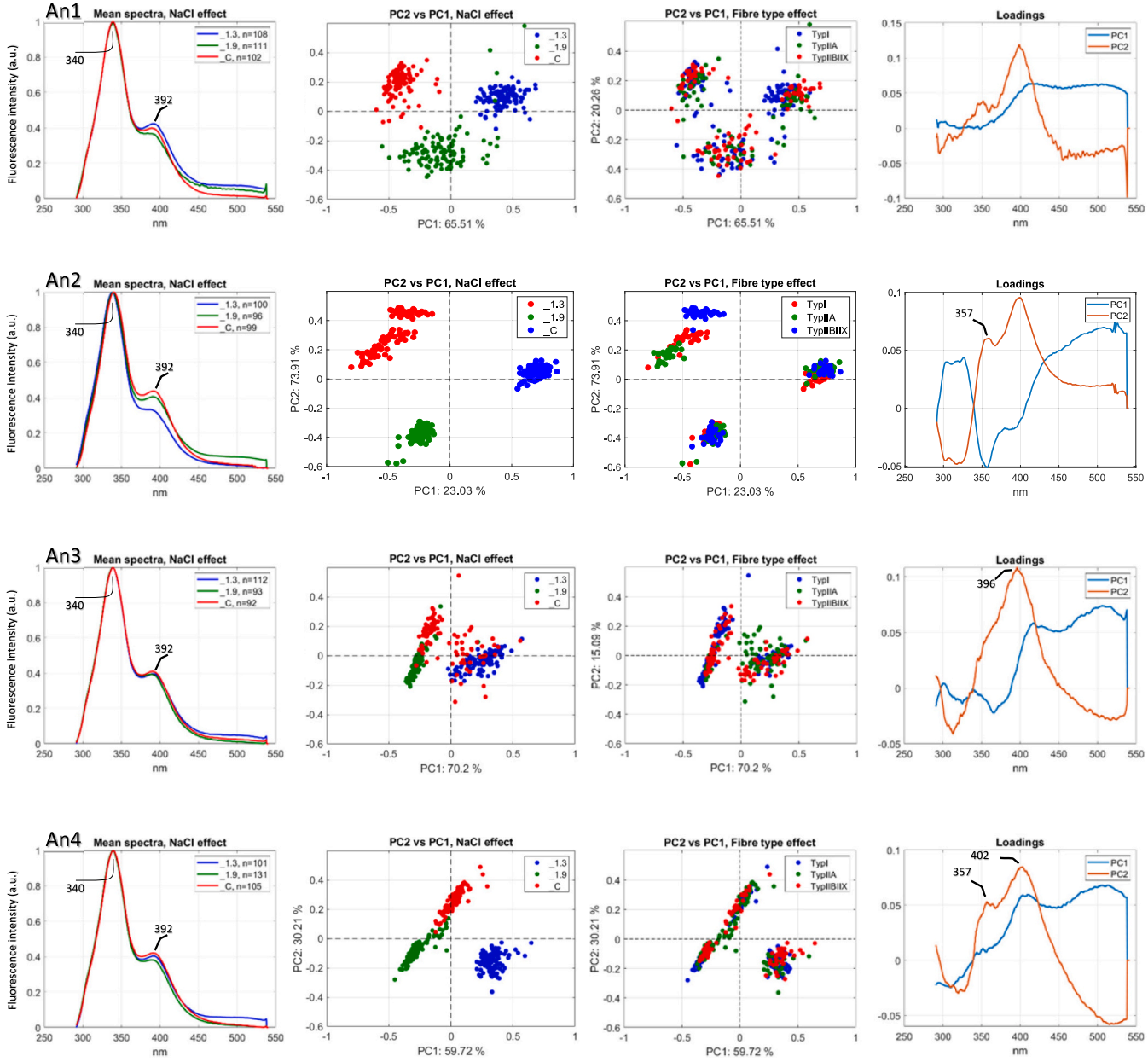

Fig. 5. Results from salt treated samples of individual animals. The 1st column presents normalised mean spectra according to NaCl levels. PCA scatter plots, according to the NaCl and fibre type factors, using data of 3 NaCl concentrations and the 3 muscle fibre types for each of the 4 animals are in columns 2 and 3 respectively. In column 4, PCA loadings are plotted for the two first components (PC1 & PC2).

(Fig. SD4) subjected to an identical salting process and analysed with a laboratory UV spectrometer (Abou El Karam et al., 2023). In this experiment, the PCA nevertheless made it possible to separate the salt levels but on the basis of variation in tryptophan autofluorescence. In the present experiment, the Synchrotron beam light enabled the highlighting of a peak of fluorescence emission around 400 nm and variations of autofluorescence in the 400–550 nm zone which are predominant in the separation of salt levels. Unfortunately, as in our previous work on ground meat (Abou El Karam et al., 2023), no simple proportionality relationship could be established to link variations in fluorescence emission and salt levels.

4. Conclusion

The study aimed to investigate the effect of salting on the autofluorescence of muscle fibres previously identified according to their type following a deep UV excitation. To do so, muscle histological sections were analysed by deep UV fluorescence microspectroscopy at the SOLEIL Synchrotron. The excitation of the muscle at 275 nm caused an intense intrinsic fluorescence emission of tryptophan with a maximum at 340 nm instead of 332 nm (which is mostly observed on muscle tissue). It also caused a fluorescence emission close to 395 nm which could be attributed to the presence of pyridoxine and/or dityrosine photochemically catalysed under UV excitation. Unlike a previous study on rat muscle, the fluorescence emission was not dependent on the fibre subtype, except for one animal whose ultimate pH was high, regardless of the salting rate. Generally speaking, the spectrofluorometry analysis on a sampling of several individuals does not make it possible to discriminate the salt levels in the muscle as a significant interindividual effect was observed. On the other hand, salt levels were properly separated on PCA of individual animals. This result indicates that individual variability overrides the effect of salting on fluorescence emission. This

result is nevertheless encouraging because it suggests that by refining the methodological approach, we can in the future identify the salt level by a spectrofluorometry measurement. Access to the wavelength continuum provided by the Synchrotron allowed us to identify the excitation wavelengths that reveal protein denaturation under the effect of salt. Thus, in the future, laser beams based on these wavelengths of interest could be used in the meat industry to characterize meat during and after the salting process. However, although separated on the PCAs of individuals, the fluorescence emission/salt content relationship does not respond to a simple prediction law, as observed with results previously obtained on ground muscle. This result leads us to say that the fluorescence emission of muscle fibres from pig muscle, at least when tumbled, is barely dependent on their metabolic and contractile type. However, it seems that the physicochemical characteristics of the muscle, and in particular its amplitude of *postmortem* pH drop, can modulate the fluorescence emission response of cell types. Further studies are necessary to confirm this hypothesis and to better understand the mechanisms involved.

Funding

This work was supported by the TRANSFORM Division of INRAE by providing a financial funding (ANS Focale) and the SOLEIL Synchrotron.

CRediT authorship contribution statement

Saïd Abou El Karam: Writing – original draft, Supervision, Software, Project administration, Methodology, Funding acquisition, Data curation. **Anne Duconseille:** Writing – review & editing, Formal analysis. **Annie Vénien:** Resources, Data curation. **Christine Ravel:** Resources, Data curation. **Hugo Chauvet:** Writing – review & editing, Resources, Funding acquisition, Data curation. **Frederic Jamme:** Writing – review & editing, Resources, Funding acquisition, Data curation. **Matthieu Réfrégiers:** Writing – review & editing, Resources, Data curation. **Thierry Astruc:** Writing – review & editing, Conceptualization.

Declaration of competing interest

The authors declare that they have no known competing financial interests or personal relationships that could have appeared to influence the work reported in this paper.

Acknowledgements

The authors thank O. Loison (INRAE), A. Vautier, M. Carlier & J. L. Martin (IFIP) for their help in muscle sample preparation.

We warmly thank our colleagues at the Synchrotron SOLEIL for their help in carrying out the measurements in the frame of the project 20191146 (Standard Proposal).

Appendix A. Supplementary data

Supplementary data to this article can be found online at https://doi.org/10.1016/j.foodchem.2025.142801.

Data availability

Data will be made available on request.

References

Abou El Karam, S., Ferrand, M., El Jabri, M., Vautier, A., Carlier, M., Germond, A., & Astruc, T. (2023). Influence of sodium chloride on muscle UV autofluorescence characteristics. *Food Chemistry, 410*, Article 135352. https://doi.org/10.1016/j.foodchem.2022.135352

Adzitey, F., & Nurul, H. (2011). Pale soft exudative (PSE) and dark firm dry (DFD) meats: Causes and measures to reduce these incidences-a mini review. *International Food Research Journal, 18*(1).

Astruc, T., Talmant, A., Fernandez, X., & Monin, G. (2002). Temperature and catecholamine effects on metabolism of perfused isolated rabbit muscle. *Meat Science, 60*(3), 287–293. https://doi.org/10.1016/S0309-1740(01)00136-X

Astruc, T., & Terlouw, E. M. C. (2023). Towards the use of on-farm slaughterhouse. *Meat Science, 205*, Article 109313. https://doi.org/10.1016/j.meatsci.2023.109313

Bailey, A. J., & Light, N. D. (1989). *Connective tissue in meat and meat products*. Elsevier.

Bendall, J. R. (1973). *Post mortem changes in muscle (H. Bourne, pp. 243–309). New York: Academic Press*.

Böcker, U., Ofstad, R., Bertram, H. C., Egelandsdal, B., & Kohler, A. (2006). Salt-induced changes in pork Myofibrillar tissue investigated by FT-IR microspectroscopy and Light microscopy. *Journal of Agricultural and Food Chemistry, 54*(18), 6733–6740. https://doi.org/10.1021/jf060178q

Chagnot, C., Vénien, A., Jamme, F., Réfrégiers, M., Desvaux, M., & Astruc, T. (2015). Hyperspectral deep ultraviolet autofluorescence of muscle fibers is affected by postmortem changes. *Journal of Agricultural and Food Chemistry, 63*(19), 4782–4789. https://doi.org/10.1021/acs.jafc.5b00668

Chagnot, C., Venien, A., Peyrin, F., Jamme, F., Refregiers, M., Desvaux, M., & Astruc, T. (2015). Deep UV excited muscle cell autofluorescence varies with the fibre type. *Analyst, 140*(12), 4189–4196. https://doi.org/10.1039/c5an00172b

Curry, A. M., Fernàndez, R. D., Pagani, T. D., Abeyawardhane, D. L., Trahan, M. L., & Lucas, H. R. (2020). Mapping of Photochemically-derived Dityrosine across Fe-bound N-acetylated α-Synuclein. *Life, 10*(8), 8. https://doi.org/10.3390/life10080124

Dancker, P., & Hasselbach, W. (1971). Dependence of actomyosin ATPase activity on ionic strength and its modification by thiol group substitution. *FEBS Letters, 16*(4), 272–274.

Dubreil, L., Damane, N., Fleurisson, R., Charrier, M., Pichon, J., Leroux, I., Schleder, C., Ledevin, M., Larcher, T., Jamme, F., Puentes, J., & Rouger, K. (2023). Specific and label-free endogenous signature of dystrophic muscle by synchrotron deep ultraviolet radiation. *Scientific Reports, 13*(1), 1. https://doi.org/10.1038/s41598-023-37762-1

Duconseille, A., Gaillard, C., Santé-Lhoutellier, V., & Astruc, T. (2018). Molecular and structural changes in gelatin evidenced by Raman microspectroscopy. *Food Hydrocolloids, 77*, 777–786. https://doi.org/10.1016/j.foodhyd.2017.11.020

Egelandsdal, B., Martinsen, B. K., Fretheim, K., Pettersen, M., & Harbitz, O. (1994). Myosins from red and white bovine muscles: Differences measured by turbidimetric, calorimetric and rheological techniques. *Journal of the Science of Food and Agriculture, 64*(1), 75–85. https://doi.org/10.1002/jsfa.2740640112

European Commission. (2013). European Commission decision of 14 November 2006 authorising methods for grading pig carcasses in France (notified under document number C (2006) 5400) (only the French text is authentic) (text with EEA relevance) (2006/784/EC). http://data.europa.eu/eli/dec/2006/784/2013-06-13/eng.

Giuliani, A., Jamme, F., Rouam, V., Wien, F., Giorgetta, J.-L., Lagarde, B., Chubar, O., Bac, S., Yao, I., Rey, S., Herbeaux, C., Marlats, J.-L., Zerbib, D., Polack, F., & Réfrégiers, M. (2009). DISCO: A low-energy multipurpose beamline at synchrotron SOLEIL. *Journal of Synchrotron Radiation, 16*(6), 6. https://doi.org/10.1107/S0909049509034049

Graiver, N., Pinotti, A., Califano, A., & Zaritzky, N. (2006). Diffusion of sodium chloride in pork tissue. *Journal of Food Engineering, 77*(4), 910–918. https://doi.org/10.1016/j.jfoodeng.2005.08.018

Guth, L., & Samaha, F. J. (1969). Qualitative differences between actomyosin ATPase of slow and fast mammalian muscle. *Experimental Neurology, 25*(1), 138–152. https://doi.org/10.1016/0014-4886(69)90077-6

Huggins, T. G., Wells-Knecht, M. C., Detorie, N. A., Baynes, J. W., & Thorpe, S. R. (1993). Formation of o-tyrosine and dityrosine in proteins during radiolytic and metal-catalyzed oxidation. *Journal of Biological Chemistry, 268*(17), 12341–12347. https://doi.org/10.1016/S0021-9258(18)31395-4

Jamme, F., Kascakova, S., Villette, S., Allouche, F., Pallu, S., Rouam, V., & Réfrégiers, M. (2013). Deep UV autofluorescence microscopy for cell biology and tissue histology. *Biology of the Cell, 105*(7), 277–288. https://doi.org/10.1111/boc.201200075

Jamme, F., Villette, S., Giuliani, A., Rouam, V., Wien, F., Lagarde, B., & Réfrégiers, M. (2010). Synchrotron UV fluorescence microscopy uncovers new probes in cells and tissues. *Microscopy and Microanalysis, 16*(5), 507–514. https://doi.org/10.1017/S1431927610093852

Karim, L., & Bouxsein, M. L. (2016). Effect of type 2 diabetes-related non-enzymatic glycation on bone biomechanical properties. *Bone, 82*, 21–27. https://doi.org/10.1016/j.bone.2015.07.028

Kato, Y., Kitamoto, N., Kawai, Y., & Osawa, T. (2001). The hydrogen peroxide/copper ion system, but not other metal-catalyzed oxidation systems, produces protein-bound dityrosine. *Free Radical Biology and Medicine, 31*(5), 624–632. https://doi.org/10.1016/S0891-5849(01)00623-2

Lakowicz, J. R. (2006). *Principles of fluorescence spectroscopy* (3rd ed.). Springer Science & Business Media.

Lebert, A., & Daudin, J.-D. (2014). Modelling the distribution of aw, pH and ions in marinated beef meat. *Meat Science, 97*(3), 347–357. https://doi.org/10.1016/j.meatsci.2013.10.017

Mirade, P. S., Portanguen, S., Sicard, J., De Souza, J., Musavu Ndob, A., Hoffman, L. C., … Collignan, A. (2020). Impact of tumbling operating parameters on salt, water and acetic acid transfers during biltong-type meat processing. *Journal of Food Engineering, 265*, Article 109686. https://doi.org/10.1016/j.jfoodeng.2019.109686

Monin, G., Talmant, A., & Vernin, P. (1973). Réaction à l'électronarcose et glycogénolyse post mortem chez le porc. *Annales de Zootechnie, 22*(1), 73–81.

Offer, G., & Knight, P. (1988). The structural basis of water-holding capacity in meat. Part 1: General principles and water uptake in meat processing. In R. Lawrie (Ed.), *Vol. 4. Developments in meat science* (pp. 63–171). Elsevier Applied Science.

Offer, G., & Trinick, J. (1983). On the mechanism of water holding in meat: The swelling and shrinking of myofibrils. *Meat Science, 8*(4), 245–281. https://doi.org/10.1016/0309-1740(83)90013-X

Réfrégiers, M., Wien, F., Ta, H.-P., Premvardhan, L., Bac, S., Jamme, F., Rouam, V., Lagarde, B., Polack, F., & Giorgetta, J.-L. (2012). DISCO synchrotron-radiation circular-dichroism endstation at SOLEIL. *Journal of Synchrotron Radiation, 19*(5), 831–835.

Ruusunen, M., & Puolanne, E. (2005). Reducing sodium intake from meat products. *Meat Science, 70*(3), 531–541. https://doi.org/10.1016/j.meatsci.2004.07.016

Sahar, A., Boubellouta, T., Portanguen, S., Kondjoyan, A., & Dufour, É. (2009). Synchronous front-face fluorescence spectroscopy coupled with parallel factors (PARAFAC) analysis to study the effects of cooking time on meat. *Journal of Food Science, 74*(9), E534–E539. https://doi.org/10.1111/j.1750-3841.2009.01365.x

Terlouw, E. M. C., Picard, B., Deiss, V., Berri, C., Hocquette, J.-F., Lebret, B., … Gagaoua, M. (2021). Understanding the determination of meat quality using biochemical characteristics of the muscle: Stress at slaughter and other missing keys. *Foods, 10*(1), 1. https://doi.org/10.3390/foods10010084

Ushijima, Y., Nakano, M., & Goto, T. (1984). Production and identification of bityrosine in horseradish peroxidase-H2O2-tyrosine system. *Biochemical and Biophysical Research Communications, 125*(3), 916–918. https://doi.org/10.1016/0006-291X(84)91370-6

Valeur, B., & Berberan-Santos, M. (2001). *Molecular fluorescence: Principles and applications*. Wiley-VCH Verlag GmbH.

Vivian, J. T., & Callis, P. R. (2001). Mechanisms of tryptophan fluorescence shifts in proteins. *Biophysical Journal, 80*(5), 2093–2109. https://doi.org/10.1016/S0006-3495(01)76183-8

Waykole, P., & Heidemann, E. (1976). Dityrosine in collagen. *Connective Tissue Research, 4*(4), 219–222. https://doi.org/10.3109/03008207609152224

Wu, F. Y., & Smith, S. B. (1987). Ionic strength and Myofibrillar protein Solubilization. *Journal of Animal Science, 65*(2), 597–608. https://doi.org/10.2527/jas1987.652597x

Wu, Z., Bertram, H. C., Kohler, A., Böcker, U., Ofstad, R., & Andersen, H. J. (2006). Influence of aging and salting on protein secondary structures and water distribution in uncooked and cooked pork. A combined FT-IR microspectroscopy and 1H NMR Relaxometry study. *Journal of Agricultural and Food Chemistry, 54*(22), 8589–8597. https://doi.org/10.1021/jf061576w

Xiong, Y. L. (1994). Myofibrillar protein from different muscle fiber types: Implications of biochemical and functional properties in meat processing. *Critical Reviews in Food Science and Nutrition, 34*(3), 293–320. https://doi.org/10.1080/10408399409527665